Particle Accelerators, 1994, Vol. 47, pp. 171–189
Reprints available directly from the publisher
Photocopying permitted by license only

PROGRESS IN LOW BETA, LOW *q/A* RFQ'S AT INS

N. TOKUDA

Institute for Nuclear Study, University of Tokyo,
Tanashi, Tokyo 188, Japan

(Received 29 October 1993)

Two split coaxial RFQ's (SCRFQ's) are presented. Both operate at 25.5 MHz and accelerate ions with a charge-to-mass ratio q/A greater than 1/30. One SCRFQ is a prototype (0.9 m diameter, 2.1 m length, 45 keV/u output energy), and the other is its extended version (0.9 m, 8.6 m, 172 keV/u). The prototype was constructed in 1989 and underwent rf and acceleration tests for two years. Through experience obtained with the prototype SCRFQ, we are now constructing the longer machine. The cavity construction is to be finished in the spring of 1994. The new SCRFQ will be used as the front-end linac in the E-Arena Test Facility, now under construction in INS. In the facility radioactive nuclei will be accelerated by the SCRFQ and an interdigital-H linac (the output energy is variable in a range of 172 through 1046 keV/u) and delivered to nuclear physics experiments.

KEY WORDS: Radio-frequency quadrupole linac, split coaxial resonator, multi-module structure, heavy ions, radioactive nuclei

1 INTRODUCTION

Split coaxial RFQ's (SCRFQ's) have been developed at INS since 1984. In this paper two SCRFQ's, which operate at 25.5 MHz and accelerate ions with a charge-to-mass ratio q/A greater than 1/30, are presented. One SCRFQ is a prototype (the length is 2.1 m, and the output energy is 45 keV/u),[1] and the other is its extended version (8.6 m, 172 keV/u).

Our SCRFQ structure is featured by modulated vanes, same as the ones used in the four-vane RFQ, and a multi-module structure.[2] This structure was devised so that we could diminish the defect of the split coaxial resonator: the inner electrodes are cantilevers, and therefore the electrodes are not firm. In the multi-module structure, however, each electrode is supported at a few points. At the prototype SCRFQ, for instance, the whole cavity (2.1 m long) comprises three module cavities (0.7 m long each), but the vanes are bars with the whole length of 2.1 m. Each vane is fixed at two points: one vane end is fixed to a cavtiy end wall, and at a point 1.4 m apart from it, the vane is supported by a stem. Since the length of the cantilever part is only 0.7 m, the electrodes are mechanically stable. Moreover, owing to the vanes with the whole length, it is easier to align the vanes precisely.

The prototype SCRFQ was constructed in 1989. Through rf and beam tests for two years, we gained confidence in our SCRFQ structure, and decided to build a longer machine. The long SCRFQ, in which the prototype is included, is now under construction, to be completed

in the spring of 1994. The new SCRFQ is to be used as the front-end linac in the E-Arena Test Facility. In this facility, radioactive nuclei will be accelerated by the SCRFQ and an interdigital-H linac.[3–7] The output beam, whose energy is fully variable in a range of 172 $\sim$ 1046 keV/u, is used for nuclear physics experiments.

This paper describes the experience obtained with the prototype SCRFQ and the design of the long SCRFQ.

2 PROTOTYPE SCRFQ

2.1 *Summary of Obtained Results*

Main parameters of the prototype SCRFQ are listed in Table 1. Through the construction and operation of the prototype SCRFQ, we obtained the following results. Concerning cavity and rf aspects, (1) the vane alignment was accurate within ± 40 μm; (2) the quadrant field balance was better than $\pm 0.7\%$ at any axial position; (3) the intervane voltage was flat over the vane length; (4) an intervane voltage of 118 kV, or a field strength of 190 kV/cm, was achieved; and (5) a 20% duty factor was possible with a peak power of 80 kW generating an intervane voltage of 109 kV. As for beam dynamics, (6) the vane-tip geometry is such that the transverse radius of curvature ρ_T is equal to r_0 ; for $\rho_T = r_0$ vanes, it is indispensable to correct the aperture radius a and modulation index m so that the corrected A_{10} coefficient might be equal to the A coefficient of the two-term potential function; and (7) the longitudinal beam dynamics in the radial matching section is not yet clear, and hence we must figure out the field distribution by using a three-dimensional field solver. Detailed descriptions on these results are presented below.

2.2 *Cavity Structure*

The structure of the prototype SCRFQ is shown in Figure 1, and the conceptual diagram of the resonator in Figure 2. The whole cavity comprises three module cavities, each of which is 0.9 m in inner diameter and 0.7 m in length. The modulated vanes, which are one-body bars of 2.1 m long, are fixed to back plates.

The materials for the cavtiy parts are as follows: (1) mild steel with 100-μm-thick copper plating for the cavity cylinder and end walls, (2) oxygen-free copper for the back plates and the stem flanges, (3) copper-plated stainless steel for the spacing rods, and (4) chromium-copper alloy (1% Cr + 99% Cu) for the vanes. Three different types of rf contanctors are used: (1) silver-plated stainless tubes (3.28 mm in diameter) between tank cylinders, (2) copper strips (1 mm $\times$ 26 mm cross section) between a stem flange and a tank cylinder, (3) shield spirals between a stem flange and a spacing rod. No contactor is inserted between a vane and a back plate.

The inner structure of the cavity was assembled outside the tank and built into the tank. The parts are bolted together. First, the stem flanges and the spacing rods were connected together into a frame, then the back-plates and the vanes were attached. For inspection of vane alignment, the interior assembly was set on a table; by the use of a dial gauge, vane positions were measured from a horizontal reference plane and a vertical one. The vane-alignment errors were less than ± 40 μm, as shown in Figure 3.

TABLE 1: Main parameters of the prototype SCRFQ.

Frequency (f)	25.5 MHz	λ = 11.76 m
Charge-to-mass ratio (q/A)	$\geq$ 1/30	
Input energy (T_{in})	1 keV/u	β = 0.00146
Output energy (T_{out})	45.4 keV/u	β = 0.00984
Normalized emittance (ε_n)	0.06 π cm·mrad	ε = 41.1 π cm·mrad (input)
Vane length (L_v)	213.5 cm	
Number of cells (N_c)	136	34 cells in radial matcher
Intervane voltage (V_{vv})	109.3 kV	q/A = 1/30 ions
Maximum surface electric field (E_s)	176.2 kV/cm	2.47 Kilpatrick (κ_{max} = 1.525)
Mean bore radius (r_0)	0.9458 cm	
Minimum bore radius (a_{min})	0.5214 cm	
Margin of bore radius (a_{min}/a_{beam})	1.2	zero-current beam
Maximum modulation index (m_{max})	2.50	
Final synchronous phase (ϕ_f)	$-30°$	
Focusing strength (B)	6.0	
Maximum defocusing strength (Δ_b)	-0.20	

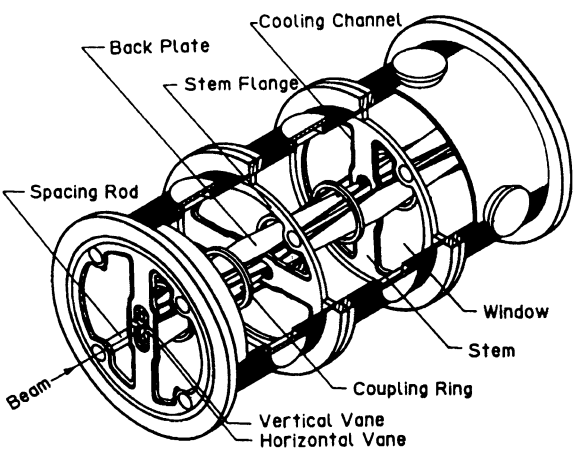

FIGURE 1: Structure of the prototype SCRFQ (25.5 MHz, 0.9 m in diameter, 2.1 m in length, three module-cavities).

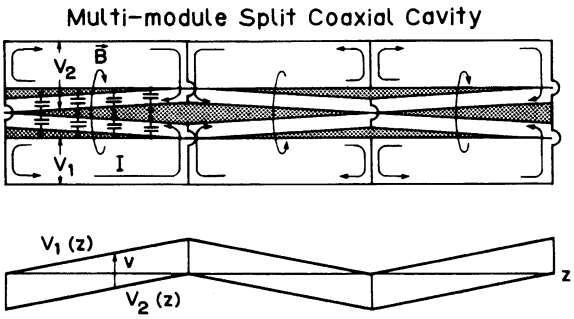

FIGURE 2: Conceptual diagram of a three-module split coaxial resonator.

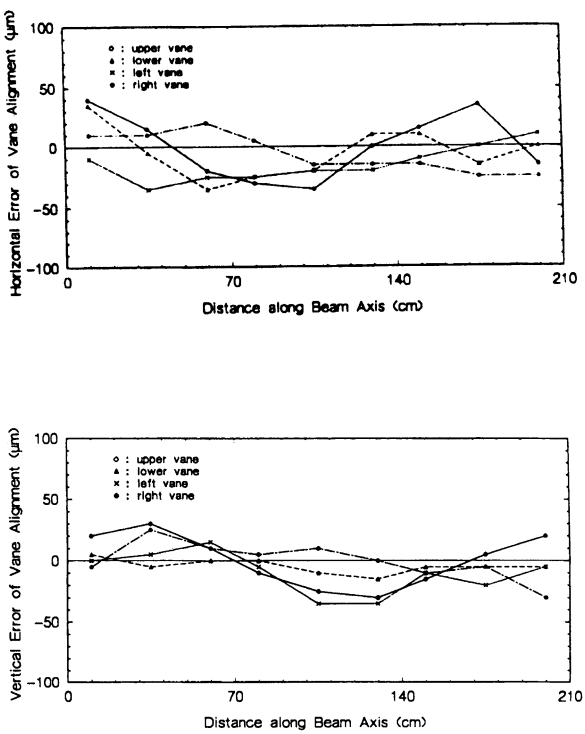

FIGURE 3: Vane-alignment errors in the horizontal and the vertical directions (top and bottom figures, respectively) measured before the inner electrode was built in the tank.

2.3 Low-power tests

The resonant frequency of the cavity was first tuned roughly to 25.45 MHz by adjusting the window areas of the stem flanges (see Figure 1), *i.e.*, we controlled the inductances associated with the magnetic fluxes around the stems.[8] Initially the windows were closed with plates with a half-moon shape; the resonant frequency measured 28.88 MHz. Then the plates were removed one by one. At every removal, the frequency decreased by 1.1 MHz, and finally reached 24.68 MHz. This meant the windows should be almost open for the frequency of 25.45 MHz. Hence we bolted copper strips along the stems; the stem width of 12 cm was thereby increased to 21 cm. For further fine tuning to 25.5 MHz, we used three inductive tuners, one tuner per module cavity. The tuners are copper cylinders, driven by stepping motors. The adjustable frequency range was about 50 kHz. The unloaded Q-value measured at 25.5 MHz is 6400, about 84% of a calculated value.

The azimuthal field balance was tested by pulling a cylindrical teflon bead (20 mm diameter, 10 mm length) down each quadrant.[9] The bead was set between neighboring vanes so that it touched them. Figure 4 shows the obtained phase shifts, approximately proportional to the square of the field amplitude. Four curves corresponding to the quadrants are drawn. The field strengths in the quadrants are balanced so well that the four curves are overlapped. We obtained $|\delta_i(z)| \leq 0.67\%$ at any axial position z, defining alignment error as $\delta_i(z) \equiv E_i(z)/\overline{E}(z) - 1$, where $E_i(z)$ is the field amplitude in the i-th quadrant, and $\overline{E}(z) = \frac{1}{4}\sum E_i(z)$.

The curves in Figure 4 are almost flat, except for three small dips at ends of the modules. The dips are due to stems, enhancing the field strength at the bead position. Such dips were not observed in another measurement by setting a bead (teflon cylinder, 0.95 cm diameter, 0.75 cm length) on the beam axis and pulling it down. The thick line in Figure 5 indicates the experimental result.[9] The thin line was obtained by a calculation under assumptions that the electric field is same as the one derived from the two-term potential function (Equation 1, Section 2.4.2), and that the intervane voltage is constant over the vane length. From this result and the flat curves in Figure 4, we conclude the distribution of the intervane voltage is flat.

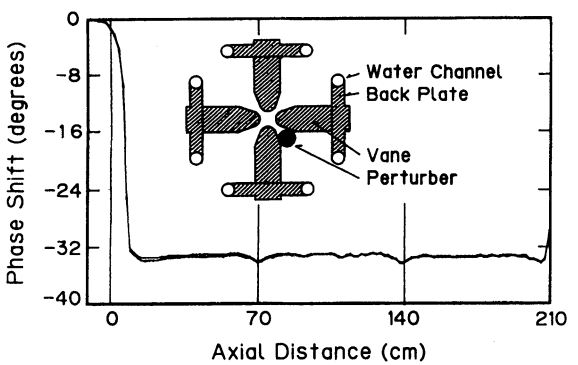

FIGURE 4: Measured field strengths (approximately $\propto$| phase shift $|^{1/2}$) between neighboring vanes. Four curves for the quadrants are plotted.

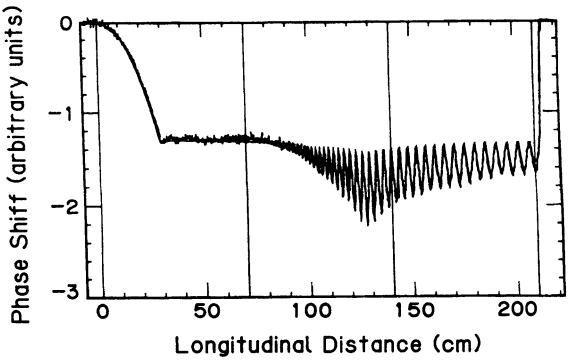

FIGURE 5: Field strengths in the beam aperture; the thick line indicates a measured strength, and the thin line a calculated one.

2.4 *High-power tests*

The driving rf power is fed to the cavity through a loop coupler (9 cm × 20 cm). The loop is rotatable for the impedance matching to 50 Ω; a VSWR of 1.01 was obtained by rotating the loop by 19° to the magnetic flux. The power source with an Eimac 4CW30000A tube has a peak power of 100 kW at maximum. The maximum duty factor at this power is 20%. The rf power is transmitted to the loop coupler through a 5.9-m-long WX-120D coaxial line.

The intervane voltage is derived from the signal from a monitor loop.[9] The calibration constant was obtained as follows. We applied directly voltage between neighboring vanes by connecting them to a signal generator with a cable, and measured the output voltage from the monitor loop. The resulting monitor loop voltage against an intervane voltage of 1 V was 0.1225 mV.

During the initial conditioning of the cavity, we increased the input power step by step with duty factors of 0.6 ~ 3%. Figure 6 shows the progress in the attained intervane voltage. After an aging time (operation time × duty factor) of 2.5 hours, we obtained 110 kV.[9] Further aging put the cavity into stable operation at higher intervane voltages and duty factors. Figure 7 shows a process that the sparking frequency decreased with time during a conditioning with an intervane voltage of 114 kV and a duty factor of 2%.[10] At a higher duty factor of 9%, we attained an intervane voltage of 118 kV. Using a field enhancement factor of 1.525 given by Crandall,[11] we estimate the highest surface field to be 190 kV/cm (2.7 Kilpatrick).

The shift of the resonant frequency was measured as a function of the average input power; the duty factor was 10% and the repetition rate was 100 Hz.[12] The result is indicated with dots in Figure 8. The resonant frequency, 25.480 MHz initially, increased to 25.608 MHz (Δf = 128 kHz) at a power of 8.5 kW and an intervane voltage of 112.7 kV. The observed frequency shift was unexpectedly large; this was due to the coupling rings. As shown in

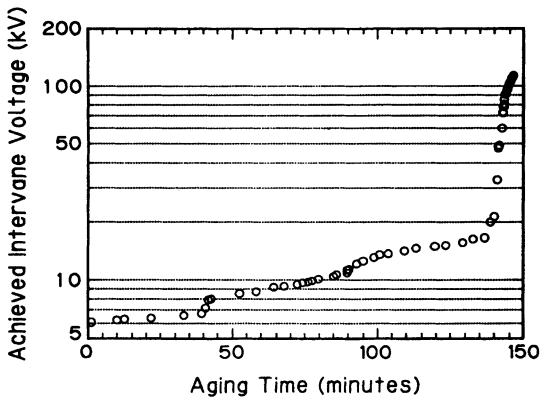

FIGURE 6: Attained intervane voltage as a function of the aging time (operation time × duty factor) during the initial rf conditioning.

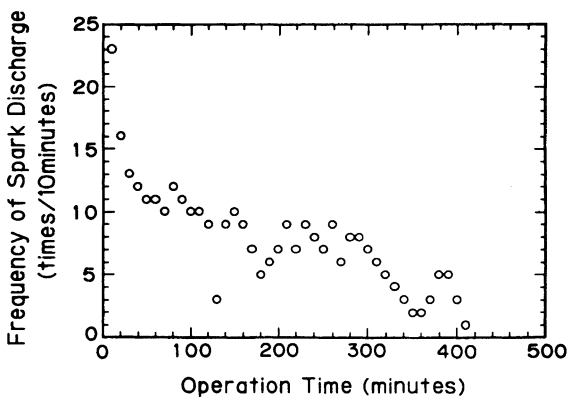

FIGURE 7: Reduction of spark discharge frequency during an rf conditioning with an intervane voltage of 114 kV and a duty factor of 2%.

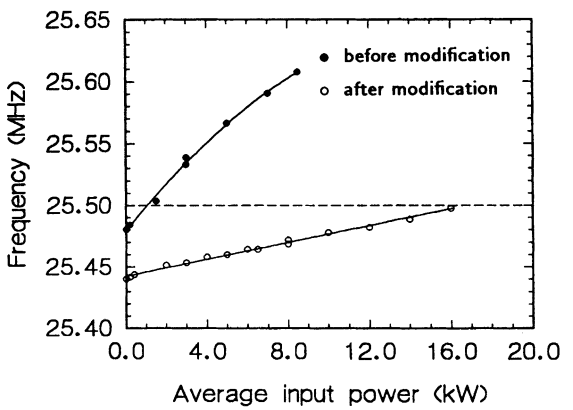

FIGURE 8: Shifts of resonant frequency *vs.* average input power, before and after the modification of the coupling rings.

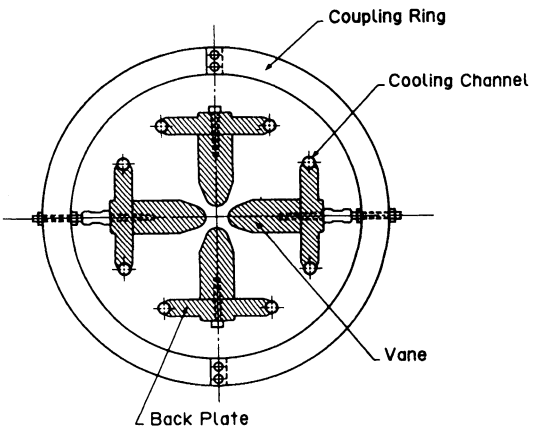

FIGURE 9: Coupling ring, fixed to back plates. The ring comprises two arcs bolted together.

Figure 9, they are fixed to diametrically opposed back plates. Since the rings are not cooled by water, they expanded under the high-power operation and pulled apart the vanes. As a result the intervane capacitance decreased, and the resonant frequency increased.

In order to reduce the frequency shift, we modified the coupling rings and re-measured the frequency shift. A coupling ring is composed of two arcs bolted together at places 90° apart from the rods connecting the arcs to the back plates. We removed the bolts and turned the arcs on the rods in opposite directions. The vanes became thereby free of the force from the coupling rings. In the frequecny-shift measurement, the cavity was operated at a 10% duty (100 Hz) for average powers lower than 8 kW; for higher powers, the peak power was kept at 80 kW (intervane voltage = 109.3 kV), and the repetition rate was increased up to a duty factor of 20%. The open circles in Figure 8 are the frequency shifts after the ring modification; the frequency shift were suppressed appreciably. The initial frequency was 25.44 MHz, lower by 40 kHz than that before the ring modification. This frequency decrease is due to the increase of the capacitance between the back plates and the turned arcs. The resonant frequency was 25.47 MHz (Δf = 29 kHz) at an average power of 8 kW, and at 16 kW, 25.50 MHz (Δf = 56 kHz).

The resonant frequency is stabilized by using the three inductive tuners, which are driven by stepping motors. In the feedback loop the stepping motors receive the phase difference between the driving rf and the picked-up signal from the monitor loop. A frequency stabilization within ±200 Hz has been obtained under an operation with an average power of 12 kW (60 kW × 20%).

From the frequency-shift measurements, we found that the coupling rings are harmful. From this experience and the observations described below, we consider that the coupling rings should be removed.[a] The purpose of the rings was to gain a better vane alignment. During the inspection of the vane alignment, however, we found that the coupling rings received no force from the back plates; this means that the vanes could have been aligned

[a] No coupling ring is used in the long SCRFQ under construction.

well enough without the coupling rings. Moreover, we conducted beam tests with the disconnected coupling rings and verified that good beam performances were obtained. The test issues were as follows: (1) transverse emittance profiles of the output beam at various intervane voltages (N^+ beam, maximum P_{ave} = 5.9 kW), (2) transmission efficiencies as a function of the intervane voltage (N^+ beam, maximum P_{ave} = 7.0 kW), and (3) transmission efficiencies as a function of the duty factor (N^+ and N_2^+ beams, maximum P_{ave} = 16.0 kW), The tests Nos.1 and 2 yielded results almost same as those with the original connected coupling rings. At the test No.3, the transmission efficiencies were independent of the duty factor.

2.5 *Acceleration Tests*

2.5.1 Introductory remarks Figure 10 shows the layout of the acceleration test stand. The ions used in acceleration tests are N_2^+, N^+, and Ne^+, which are produced in an ECR ion source. We conducted experiments on the following issues: transverse emittance and energy profiles of the output beam at various intervane voltages, transmission efficiency as a function of the intervane voltage, transmission efficiency as a function of the input energy.[12–14] The results showed that there was no problem in the transverse beam dynamics. As for the longitudinal beam dynamics, however, we have two subjects to discuss: one is the A_{10} coefficient for the $\rho_T = r_0$ vane, and the other is the beam motion in the radial matching section.

2.5.2 A_{10} coefficient In the discussion below, we use three versions of the PARMTEQ program: PARMTEQ-2, -M, and -H. In PARMTEQ-2, the electric field is derived from the two-term potential function. In PARMTEQ-M, the A coefficient of the two-term potential function is replaced with A_{10} coefficient calculated by Crandall.[11] In PARMTEQ-H, Crandall's A_{ji} coefficients are used (higher-order multipoles are included).

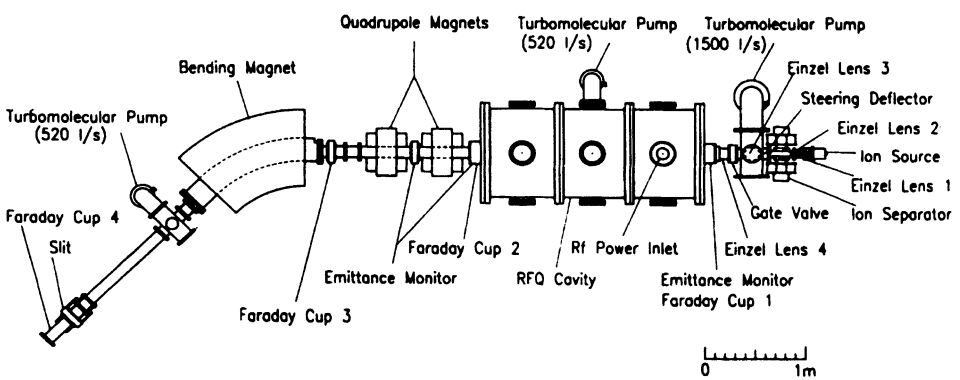

FIGURE 10: Layout of the acceleration test stand.

The two-term potential function, used in PARMTEQ-2, is expressed as:

$$U_2(r, \psi, z) = \frac{V}{2}\left[\left(\frac{r}{r_0}\right)^2 \cos 2\psi + A\, I_0(kr) \cos kz\right], \tag{1}$$

where V is the intervane voltage, $k = \pi/(\text{cell length}) = 2\pi/\beta\lambda$, and I_0 is the modified Bessel function of order zero.[15] The parameters A and r_0 are determined by the boundary conditions:

$$A = \frac{m^2 - 1}{m^2 I_0(ka) + I_0(mka)}, \quad r_0 = a\,[\,1 - A I_0(ka)\,]^{-1/2}, \tag{2}$$

where a is the minimum distance from the z-axis to the vane tip, and ma is the maximum distance. Equating the right-hand side of Equation 1 to $\pm V/2$, we have equations representing equipotential surfaces. The ideal vanes would have surfaces same as the equipotential surfaces. For technical reasons, however, the geometry of actual vanes are different from that of the ideal ones, and therefore the actual electric field will be different from that derived from the two-term potential function.

For the actual vanes, the potential function should be expressed in a more general form:

$$U(r, \psi, z) = \frac{V}{2}\left[\sum_{i=1}^{\infty} A_{0i}\left(\frac{r}{r_0}\right)^{2i} \cos 2i\psi + \sum_{i=0}^{\infty}\sum_{j=1}^{\infty} A_{ji}\, I_{2i}(jkr) \cos 2i\psi \cos jkz\right]. \tag{3}$$

From the fourth symmetry condition, if i (j) is even, then j (i) must be odd. Using a program CHARGE 3-D, Crandall calculated eight lowest-order multipole coefficients for differing vane-tip geometries: the transverse radius of curvature ρ_T is variable with respect to z, or constant (= r_0 or 0.75 r_0); the longitudinal vane profile is standard (derived from the two-term potential function) or sinusoidal.[11] He tabulates resulting A_{ji}'s for an array of the modulation index m and the cell length divided by r_0. At any geometry, the resulting coefficients, except for A_{10}'s, are close to those of the two-term potential function, *i.e.*, A_{01} is almost unity, and higher-order coefficients are small. The A_{10} coefficient is, however, appreciably different from A; particularly at the constant ρ_T vanes, the A_{10}/A ratio is about 0.6 or 0.7 in the low-energy region (short cell length and small m).

At our vanes, ρ_T is constant at r_0 = 0.946 cm, and the longitudinal vane tip profile is the standard one. We computed the A_{10}/A ratio for every cell by using an interpolation procedure on the Crandall's table values; a computer program MOD12 was used for the interpolation.[16] The resulting A_{10}/A is shown in Figure 11, along with the synchronous phase ϕ_s, design values with $A_{10} = A$. The A_{10}/A ratio is smaller than unity in the bunching process, where synchronous phase increases from $-90°$ to $-30°$. According to the PARMTEQ-2 simulation with $A_{10} = A$, many ions lie near the separatrix during the bunching process. If $A_{10} < A$, the separatrix shrinks both in phase width and energy height; as a result, some particles will spill from the rf bucket, and the transmission efficiency will be reduced.

The expected reduction of the transmission efficiency was experimentally verified.[14] Figure 12 shows experimental and simulation results for the transmission efficiency as a function of the normalized intervane voltage V_n. The transmission efficiency is defined by

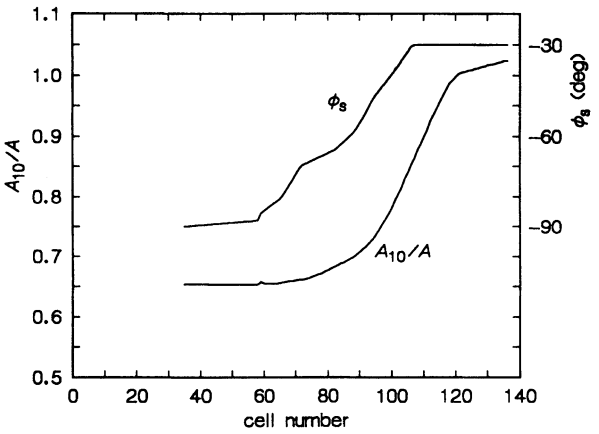

FIGURE 11: A_{10}/A ratio and the designed synchronous phase ϕ_s as functions of the cell number.

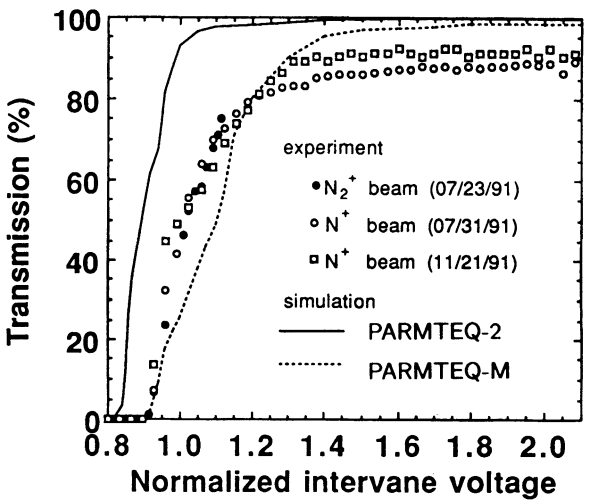

FIGURE 12: Transmission efficiencies *vs.* the normalized intervane voltage. Results of experiments and simulations are plotted.

the ratio of the current of accelerated ions to that of the injected ions, and the normalized intervane voltage by the ratio of the measured voltage to the design value. In the range of $V_n \leq 1.3$, the measured transmission efficiencies are much lower than the PARMTEQ-2 values. The result of PARMTEQ-M runs looks better; this program uses A_{10} in place of A,

and consequently yields reduced transmission efficiencies.[b] Therefore the A_{10} coefficient of the actual field will be close to the Crandall's value.[c]

The experiment shows that the A_{10} correction is indispensable to the $\rho_T = r_0$ vane. If $A_{10} < A$, A_{10} should be enhanced by correcting a and m parameters so that the A_{10} after the correction is equal to the A before the correction, and the r_0 value is preserved. This correction is carried out by using MOD12. For the five vane-tip geometries presented by Crandall,[11] their performances were compared by running PARMTEQ-H. The results are summarized in Table 2, the run No.3 ($\rho_T = r_0$, standard modulation) shows that, with the A_{10} correction, we can obtain transmission efficiencies as high as those predicted by PARMTEQ-2. This vane-tip geometry is, however, unacceptable because the minimum longitudinal radius of curvature $\rho_{L,min}$ of the vane tip is too small. At the vane-tip machining by means of the two-dimensional cutting technique with a shaped cutter, $\rho_{L,min}$ must be larger than the cutter radius (= the distance from the axis of rotation to the upper edge of the cutting surface). In our case, the cutter radius is 1.00 cm, which was determined so that the cutter might be strong enough. The $\rho_{L,min}$ before the A_{10} correction is 1.056 cm (Nos.1 and 2 in Table 2), but after the correction, the radius is no more than 0.66 cm (No.3). Employing the sinusoidal modulation, we can avoid the $\rho_{L,min}$ problem. Hence the vane-tip geometry of $\rho_T = r_0$, sinusoidal modulation (No.4) would be the right geometry for the prototype SCRFQ.

TABLE 2: Transmission efficiencies (beam current is 0 or 5 mA, q/A = 1/30) and minimum longitudinal radii of curvature $\rho_{L,min}$ for various vane-tip geometries. At PARMTEQ-M, no A_{10} correction is made, and no higher-order multipole is included. At PARMTEQ-H, the correction is made, and all of the Crandall's higher-order multipoles are included.

No.	Program	ρ_T	Modulation	$\rho_{L,min}$	Tr.(0 mA)	Tr.(5 mA)
1	PARMTEQ-2		standard	1.056 cm	92.6%	47.4%
2	PARMTEQ-M	r_0	standard	1.056 cm	25.2%	16.2%
3	PARMTEQ-H	r_0	standard	0.660 cm	92.6%	45.2%
4	PARMTEQ-H	r_0	sinusoidal	1.187 cm	92.6%	47.4%
5	PARMTEQ-H	0.75 r_0	standard	0.572 cm	88.4%	37.8%
6	PARMTEQ-H	0.75 r_0	sinusoidal	1.106 cm	89.6%	40.2%
7	PARMTEQ-H	variable	standard	0.937 cm	92.6%	41.8%

[b] Transmission efficiencies provided by PARMTEQ-M are lower than the measured values in the range of $0.9 \leq V_n \leq 1.1$. This would be due to imperfect beam simulation in the radial matching section, as will be discussed later.

[c] Another computer program POT3D[17] yields A_{10}/A ratios nearly same as those by Crandall's CHARGE 3-D; the discrepancy is less than 1%.

2.4.3 Radial matching section In the PARMTEQ simulations, we assume that the electric field in the radial matching section (RMS) is derived from the following potential function:

$$U(x, y, z) = \frac{V}{2}\left[1 + \frac{x^2 - y^2}{{r_0}^2}\right]\frac{z}{L}, \tag{4}$$

where V is the intervane voltage, r_0 the aperture radius at the exit of the RMS (= mean aperture radius), and L the RMS length; at the prototype SCRFQ, r_0 = 0.9458 cm and L = 29.2 cm. Therefore the potential on the beam axis ramps from 0 to $V/2$ in the RMS, or the longitudinal component E_z of the electric field is not zero. Owing to this E_z, the energy and phase modulations that the beam experiences is quite particular: if the input beam is a d.c.beam with the design energy W_{in}, particles move toward $\Delta\phi = \pm\pi$ ($\Delta\phi \equiv$ rf phase ϕ − synchronous phase ϕ_s). Consequently, the beam is bunched, and at the exit of the RMS the particle density is minimum at $\Delta\phi = 0$, and maximum at $\Delta\phi = \pm\pi$. Particles in the peaks around $\Delta\phi = \pm\pi$ will spill from the rf bucket in the bunching process, resulting in a lower transmission efficiency. When the input energy differs slightly from W_{in}, the beam bunching takes place also. The peak position is, however, apart from $\Delta\phi = \pm\pi$, and therefore the particles in the peak will be captured well, leading to a higher transmission efficiency.

The transmission efficiency as a function of the injection energy is shown in Figure 13, where PARMTEQ-M results and experimental data are plotted.[12] The simulation results are remarkable for holes around $\Delta W_{in} / W_{in} = 0$; the holes are due to the beam bunching in the RMS. The experiment, however, denies apparently the simulation results. This implies that the beam may not be bunched in the RMS, or the actual electric field in the RMS may be different from the potential function of Equation 4.

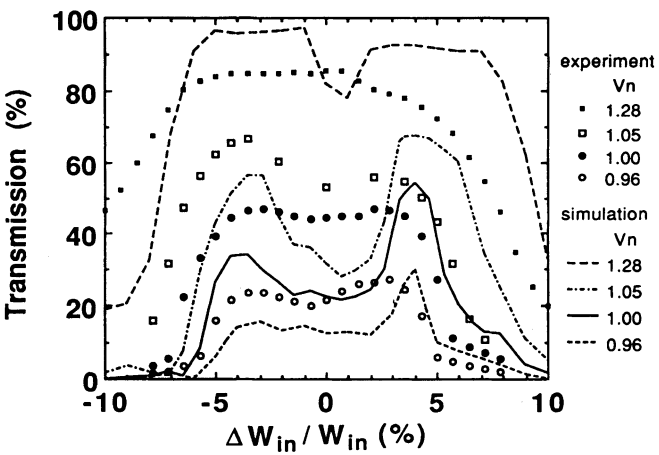

FIGURE 13: Transmission efficiency *vs.* injection energy for some values of the normalized intervane voltage V_n. The ions used in the experiments are N_2^+ (V_n = 0.96, 1.00, 1.05) and N^+ (V_n = 1.28).

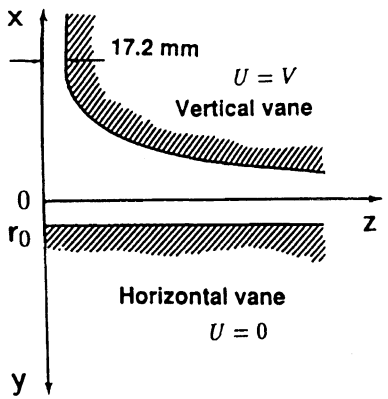

FIGURE 14: Longitudinal vane profiles in the radial matching section. At the prototype SCRFQ, r_0 = 0.9458 cm and the section length is 29.2 cm.

In our simulation E_z (here defined as $-\partial U/\partial z$) has a rectangular variation with respect to z. The abruptly ramping E_z causes the beam bunching. According to simulations, the beam bunching is very sensitive to the functional shape of E_z at the RMS entrance; if E_z varies smoothly in the RMS, no beam bunching occurs.[18] It is quite possible that the actual E_z may not have a step-like shape at the RMS entrance for the following reasons. (1) The vanes are not shaped to the the equipotential surfaces. They will be obtained by equating the right-hand-side of Equation 4 to 0 or V. The resulting transverse radii of curvature at the vane tips are:

$$\rho_T = r_0 \quad (U = 0 \text{ vanes}) , \qquad r_0 \left(\frac{2L}{z} - 1 \right)^{1/2} \quad (U = V \text{ vanes}) . \tag{5}$$

At the actual vanes, however, the vane tips are shaped to a circular arc with $\rho_T = r_0$, in the same manner for the modulated vanes. This shaping would be good for the $U = 0$ vanes, but worse for the $U = V$ vanes. (2) The $U = V$ vanes are truncated at z = 1.72 cm, since the equipotential sufaces for these vanes flare out, approaching infinitely the end wall, as shown in Figure 14. (3) The RMS entrance includes the beam hole. From the above considerations, the actual E_z may vary gently in the RMS entrance, but not ramp on abruptly. For a precise beam simulation, it is necessary to examine the field distribution in the RMS by using a three-dimensional field solver.

3 LONG SCRFQ

3.1 Radioactive Beam Facility

A prototype facility for the Exotic-Nuclei Arena (E-Arena) in the Japanese Hadron Project is now under constructione at INS.[19] In the facility, radioactive nuclei will be accelerated by linacs and used for nuclear physics experiments. The primary beam will be a 40-MeV,

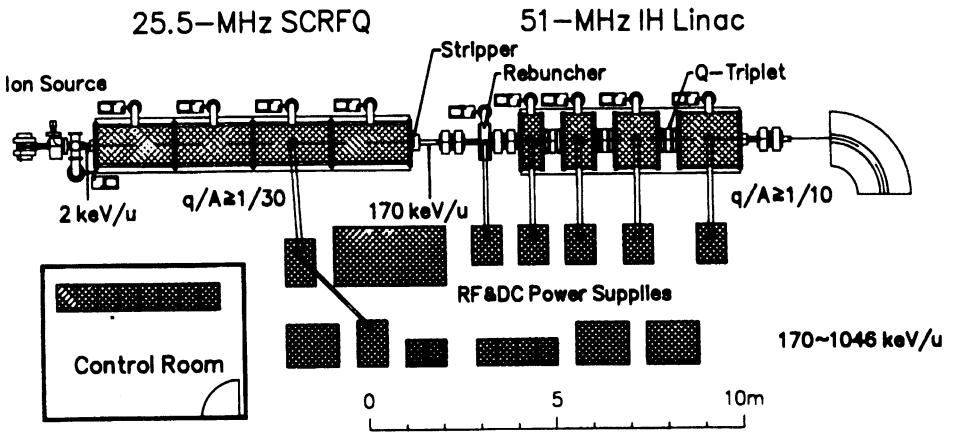

FIGURE 15: Layout of the linac chain in the E-Arena Test Facility, now under construction.

10-μA proton beam from the existing sector focusing cyclotron. Radioactive nuclei will be mass-analyzed through an isotope separator on-line (ISOL) with a mass resolution of $\Delta m/m$ = 1/9000, and transported to a linac chain, whose layout is shown in Figure 15.[3–7]

The front-end linac is a 25.5-MHz, 8.6-m SCRFQ, accelerating ions with $q/A \geq 1/30$ from 2 to 172 keV/u. A carbon-foil stripper is located at the exit of the SCRFQ; through a foil of 10 μg/cm^2 thick or less, the charge-to-mass ratio will be enhanced to $q/A \geq 1/10$. Two doublets of quadrupole magnets will be used for the transverse matching. For the longitudinal matching, a 25.5-MHz rebuncher will be used; a folded $\lambda/4$-resonator with four or six gaps is now being studied. An interdigital-H (IH) linac, consisting of four tanks and three quadrupole-magnet triplets between them, accelerates ions further. The output energy is continuously variable in a range of 172 $\sim$ 1046 keV/u. The variable energy is obtained by adjusting the rf power and phase in the last tank of operating ones.

3.2 *Design of the Long SCRFQ*

The long SCRFQ is now under construction, to be completed in the spring of 1994. It is an extend version of the prototype: the number of module cavities has been increased to 12, and the overall length is 8.6 m. Main parameters of the long SCRFQ are listed in Table 3. At the construction, the whole cavity is divided into four units (the prototype is a 1-unit cavity). Three of them are newly constructed, and the other one is the prototype with replaced vanes. The units are assembled separately and connected into the whole cavity.

For the new SCRFQ, the following improvements were made. The coupling rings have been removed, since they are harmful to high-power, high-duty operations. The flow rate of the cooling water is to be increased so that the cavity might stand a full-power operation with a duty factor of 30%. The A_{10} correction is applied to the vanes.

TABLE 3: Main parameters of the long SCRFQ.

Frequency (f)	25.5 MHz	λ = 11.76 m
Charge-to-mass ratio (q/A)	$\geq$ 1/30	
Input energy (T_{in})	2 keV/u	β = 0.00206
Output energy (T_{out})	172 keV/u	β = 0.01916
Normalized emittance (ε_n)	0.06 π cm·mrad	ε = 29.1 π cm·mrad (input)
Vane length (L_v)	858.5 cm	
Number of cells (N_c)	172	20 cells in radial matcher
Intervane voltage (V_{vv})	108.6 kV	q/A = 1/30 ions
Maximum surface electric field (E_s)	178.2 kV/cm	2.49 Kilpatrick (κ_{max} = 1.615)
Mean bore radius (r_0)	0.9846 cm	
Minimum bore radius (a_{min})	0.5388 cm	
Margin of bore radius (a_{min}/a_{beam})	1.2	zero-current beam
Maximum modulation index (m_{max})	2.53	
Final synchronous phase (ϕ_f)	$-30°$	
Focusing strength (B)	5.5	
Maximum defocusing strength (Δ_b)	-0.17	

The vane-tip geometry is as follows: ρ_T is variable in the low-energy part (up to the center of the 76th cell, 1.1 m down from the RFQ entrance), in the remaining high-energy part, $\rho_T = r_0$ (0.985 cm); the modulation is the standard one at both of the vane-tip geometries. As shown in Figure 16, the A_{10}/A curves cross at the 76th cell. Therefore, the amount of corrections for a and m are same at this cell, and the two vanes connect smoothly. The vanes in the first unit are machined by using a ball-end mill (three-dimensional cutting), and those in the other units by using a shaped cutter (two-dimensional cutting).

The connection of the two vane-tip geometries may have an advantage that the A_{12} coefficient is minimized. The pseudo-octapole field from the A_{12} term affects the beam performance more than the other higher-oder multipoles do. Without the octapole field, the shape of the beam cross section is nearly circular. The octapole field deforms the beam shape to a square, and as a result, the transmission efficiency will be decreased. We evaluate the strength of the A_{12} multipole by the following ratio:

$$R(r) = \frac{A_{12}\, I_4'(kr)}{A_{10}\, I_1(kr)}\ , \tag{6}$$

the numerator and the denominator come from A_{12} - and A_{10} -terms in the E_r derived from the potential function of Equation 3. The R-ratios at r = 0.3 cm for the two vane-tip geometries are plotted in Figure 17, along with the rf defocusing parameter Δ_{rf}, which is

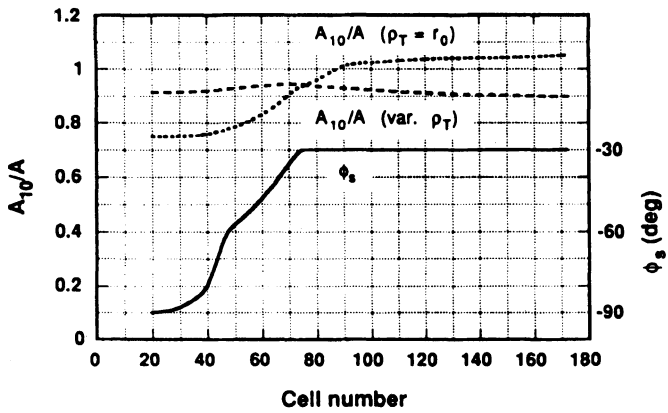

FIGURE 16: A_{10}/A ratios for the variable ρ_T vane and the $\rho_T = r_0$ one as functions of the cell number. The synchronous phase ϕ_s is also plotted.

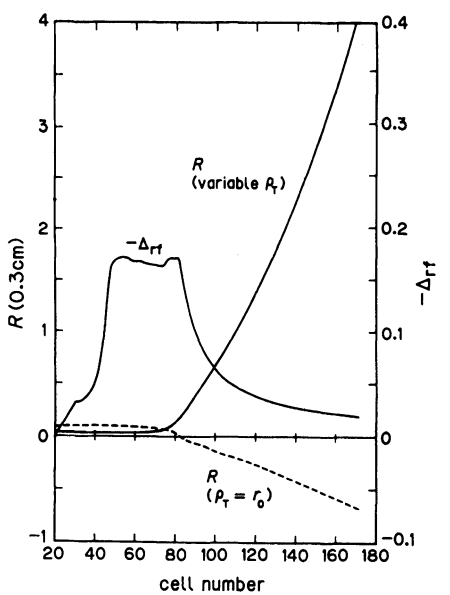

FIGURE 17: Ratios $R(r = 0.3$ cm) for the variable ρ_T vane and the $\rho_T = r_0$ one as functions of the cell number. The rf defocusing parameter Δ_{rf} is also plotted.

TABLE 4: Transmission efficiencies (beam current is 0, 5, or 10 mA, q/A = 1/30) provided by PARMTEQ-2 and those by PARMTEQ-H for various vane-tip geometries with the standard modulation. At PARMTEQ-H, the A_{10} correction is made, and all of the Crandall's higher-order multipoles are included. No beam bunching in the radial matching section is assumed.

No.	Program	Vane-tip geometry	Tr.(0 mA)	Tr.(5 mA)	Tr.(10 mA)
1	PARMTEQ-2		91.4%	87.6%	68.4%
2	PARMTEQ-H	var. $\rho_T + \rho_T = r_0$	91.4%	86.0%	65.2%
3	PARMTEQ-H	$\rho_T = r_0$	90.8%	81.8%	60.2%
4	PARMTEQ-H	variable ρ_T	90.0%	80.0%	55.0%

proportional to A_{10} . In terms of smaller A_{12} coefficient, the variable ρ_T vane is better in a low-energy part, and in a high-energy part the $\rho_T = r_0$ vane is better.

Table 4 summarizes transmission efficiencies obtained through PARMTEQ-2 runs and PARMTEQ-H ones for three vane-tip geometries: (1) variable $\rho_T + \rho_T = r_0$ vane (the geometry in our SCRFQ), (2) $\rho_T = r_0$ vane throughout, and (3) variable ρ_T vane throughout. For a zero-current beam, the three vane-tip geometries yield transmission efficiencies almost same as that by PARMTEQ-2. However, as the beam current increases, the difference becomes larger: the variable $\rho_T + \rho_T = r_0$ vane is best, and the variable ρ_T vane is worst. The effect of the A_{12} multipole becomes remarkable at high beam currents, because the beam radius is enlarged by the space charge force, and the A_{12} term in E_r is proportinal to $I_4'(kr)$, approximately $\propto r^3$. It might be overdone to connect together the two vane-tip geometries, because the SCRFQ is for a low-current beam of radioactive nuclei. The vane connection, however, will make sense, considering possible emittance growth brought about by imperfections in the vane alignment or mismatching between the input beam and the RFQ.

5 CONCLUDING REMARKS

Through the operation of the prototype SCRFQ, we verified that the SCRFQ with the multi-module structure works well and found some items to be improved for better performance. The long SCRFQ is now under construction and will be set up in INS in 1994. The rf power source with an Eimac 4CW150000E tube is ready. Its maximum peak power is 350 kW with a duty factor of 30%. The IH linac and its power sources are being constructed, to be finished in the spring of 1995. The design study on the beam transport lines and model tests on components are in process. The first beam acceleration, probably using a beam of stable nuclei, is scheduled in the fiscal year of 1995.

ACKNOWLEDGEMENTS

The development of the two SCRFQ's has been conducted by S. Arai, A.Imanishi, T. Morimoto, S. Shibuya, T. Takeda, E. Tojyo, and N. Tokuda. I wish to thank J. Staples

and S. Yamada for their help in compilation of computer programs and discussion on beam dynamics. In addition, the supports provided by M. Kihara, the Accelerator Research Division, High Energy Physics Division, and Nuclear Physics Division of INS, and by the Grant for Scientific Research of the Ministry Education, Science and Culture are gratefully acknowledged. The computer works were done on FACOM M780 in the INS Computer Room.

REFERENCES

1. S. Shibuya, "Study of an SCRFQ Linac for Very Slow Heavy-Ion Beams", thesis for Ph.D.(in Japanese), National Laboratory for High Energy Physics, KEK Internal 92–10, 1992.
2. S. Arai, "Split Coaxial RFQ Structure with Modulated Vanes", Gesellschaft für Schwerionenforschung, GSI-83-11, 1983.
3. S. Arai *et al.*, "A Heavy-Ion Linac Complex for Unstable Nuclei", IEEE 1993 Particle Accelerator Conference, Washington, D.C., USA, May 1993.
4. S. Arai *et al.*, "Construction of a Heavy-Ion Linac for Short-Lived Nuclei", 9th Symposium on Accelerator Science and Technology, Tsukuba, Japan, August 1993.
5. M. Tomizawa *et al.*, "Interdigital-H Linac for Unstable Nuclei at INS", IEEE 1993 Particle Accelerator Conference Washington, D.C., USA, May 1993.
6. M. Tomizawa *et al.*, "Development of an Interdigital-H Linac for Unstable Nuclei at INS", 5th Japan-China Joint Symposium on Accelerators for Nuclear Science and Their Applications, Osaka, Japan, October 1993.
7. K. Niki *et al.*, "Beam Matching Section in the INS Heavy Ion Linac Complex", IEEE 1993 Particle Accelerator Conference, Washington, D.C., USA, May 1993.
8. N. Tokuda *et al.*, "Structure and RF Characteristics of the INS 25.5-MHz Split Coaxial RFQ", 7th Symposium on Accelerator Science and Technology, Ibaraki, Osaka, Japan, December 1989.
9. S. Shibuya *et al.*, "RF Tests on the INS 25.5-MHz Split Coaxial RFQ", 1990 Linear Accelerator Conference, Albuquerque, NM, USA, September 1990.
10. S. Arai *et al.*, "A Split Coaxial RFQ for an ISOL Post-Accelerator", 4th China-Japan Joint Symposium on Accelerators for Nuclear Science and Their Applications, Beijing, China, October 1990.
11. K.R. Crandall, "Effects of Vane-Tip Geometry on the Electric Fields in Radio-Frequency Quadrupole Linacs", Los Alamos National Laboratory, USA, LA-9695-MS, 1983.
12. N. Tokuda *et al.*, "Performance Characteristics of the INS 25.5-MHz Split Coaxial RFQ", 3rd European Particle Accelerator Conference, Berlin, Germany March 1992.
13. S. Arai *et al.*, "Acceleration Tests of the INS 25.5-MHz Split Coaxial RFQ", IEEE 1991 Particle Accelerator Conference, San Francisco, CA, USA May 1991.
14. N. Tokuda *et al.*, "Acceleration Performance of the INS 25.5-MHz Split Coaxial RFQ", 8th Symposium on Accelerator Science and Technology, Wako, Saitama, Japan, November 1991.
15. K.R. Crandall *et al.*, "RF Quadrupole Beam Dynamics Design Studies", 1979 Linear Accelerator Conference, Montauk, NY, USA, September 1979.
16. J. Staples, private communication, May 1989.
17. S. Yamada, "3D Electric Field Caculation with Surface Charge Method", 8th Symposium on Accelerator Science and Technology, Wako, Saitama, Japan, November 1991.
18. J. Staples, private communication, September 1993.
19. I. Katayama *et al.*, "Radioactive Ion Beam Facility at INS", 3rd International Conference on Radioactive Nuclear Beams, East Lansing, MI, USA, May 1993.